

Seeing (ultra)sound in real-time through the Acousto-PiezoLuminescent lens

Mathias Kersemans¹, Simon Michels², Philippe F. Smet² and Wim Van Paepegem¹

¹ Mechanics of Materials and Structures MMS, Faculty of Engineering and Architecture, Ghent University, 9000 Gent, Belgium

² Lumilab, Faculty of Sciences, Ghent University, 9000 Gent, Belgium

ABSTRACT

In this contribution, we focus on a recently developed piezoluminescent phosphor BaSi₂O₂N₂:Eu (BaSiON), and report on Acoustically induced PiezoLuminescence (APL). Insonification of the BaSiON phosphor with (ultra)sound waves leads to intense light emission patterns which are clearly visible by the bare eye. The emitted light intensity has been measured with a calibrated photometer revealing it is directly proportional to the applied acoustic power. As such, APL can be used to devise a simple but effective acoustic power sensor. Further, the emitted APL light pattern has a specific geometrical shape which we successfully linked to the pressure field of the incident (ultra)sonic wave. This is explicitly demonstrated for an ultrasonic ($f = 3.3$ MHz) transducer. By varying the insonification distance (from near- to far-field), multiple 2D slices of the transducer's radiation field light up on the BaSiON phosphor plate. By simply photographing these light patterns, and stacking them one after another, the 3D spatial radiation field of the ultrasonic transducer was reconstructed. Good agreement was found with both classical scanning hydrophone experiments and simulations. Recently we found that APL can also be activated by acoustic waves in the kHz range, thus covering a wide frequency range. Some first preliminary results are shown.

1. INTRODUCTION

Humans have the natural ability to sense an internal or external pressure applied to the skin. As such, people can react whenever touched, and are alerted in case of danger. Few materials have a similar ability, though in a slightly different way: they emit cold-body radiation (i.e. radiation not resulting from heat according to black body physics) when stimulated by mechanical stress and are therefore termed mechanoluminescent (ML) materials. The phenomenon of ML was discovered by Sir Francis Bacon who first observed it in 1605 when scraping sugar (Bacon, 1605). Depending on the stimulating mechanical action and the degree of deformation, different names are used, including fractoluminescence, triboluminescence, and piezoluminescence. Last decades, humans have designed several novel ML materials, called phosphors, with an increased sensitivity to different mechanical stimulations (Chandra et al., 2013). As such, these phosphors have already been successfully employed for a range of interesting applications:

- sensing a dynamic (elastic) pressure by dispersing the active non-stoichiometric Sr_{0.975}Al₂O_{3.985}:Eu_{0.01} in an epoxy matrix (Xu et al., 2000), or by covering structural components with an active CaZnOS:Mn film (Zhang et al., 2013),
- assessing quasi-dynamic crack propagation (up to 15 m/s) using the fractoluminescent SrAl₂O₄:Eu,Dy phosphor (Kim et al., 2007, Timilsina et al., 2013),
- mapping personalized handwriting (Wang et al., 2015),
- determination of stress intensity factors in mode I setup (Timilsina et al., 2013) and
- detection of ultrasonic waves (Terasaki et al., 2013, Zhan et al., 2011, Zhang et al., 2013).

The phenomenon of ML is closely related to persistent luminescence or afterglow (Van den Eeckhout et al., 2010, Matsuzawa et al., 1996, Brito et al., 2012). Persistent luminescence is a specific type of luminescence where the emission is delayed for seconds up to days after the excitation, due to the presence of trap states. After excitation, charge carriers are captured in traps, often related to lattice defects or intentionally added impurities. The trapped charges are then thermally released, after which recombination at the luminescence center occurs. The thermal barrier for detrapping determines the afterglow duration, depending on the ambient temperature and the trap depth,

which can be a distribution rather than a single, discrete trap depth (Van den Eeckhout et al., 2013). The detrapping can also occur following mechanical action, although not all persistent luminescent materials show ML, which is presumably related to their crystal structure (Botterman et al., 2012). Here we use the bluish-green emitting $\text{BaSi}_2\text{O}_2\text{N}_2:\text{Eu}$ (BaSiON) phosphor which shows both persistent luminescence and ML. The emitted light has an emission peak at 498 nm (full-width-half-maximum of 32 nm), resulting from a $4f^65d-4f^7$ transition within divalent europium. BaSiON is characterized by a broad trap depth distribution and applying pressure was reported to lead to a preferential release from deep traps. Direct recombination at the ionized europium center can then occur (leading to immediate light emission), or retrapping into shallower traps, causing a short afterglow when the pressure is released (Botterman et al., 2012).

In this paper, we demonstrate that luminescence can also be triggered by acoustic waves. For the BaSiON phosphor, we actually observe intense luminescence upon insonification which is even visible with the bare eye. In the remainder of the text, we use the term Acoustically induced PiezoLuminescence or Acousto-PiezoLuminescence (APL). First, the relation between APL light intensity and applied acoustic power is investigated. Secondly, the APL phenomenon is used to reconstruct the 3D spatial radiation field of an ultrasonic transducer (frequency $f = 3.3$ MHz) in both near- and far-field (Kerseman et al., 2015). The obtained results are confronted with both scanning hydrophone experiments and 3D acoustic holography simulations, showing good comparison. Finally, preliminary results are shown, indicating that the APL phenomenon is not only useful for ultrasonic waves with MHz frequency, but can also be activated in the acoustic kHz range.

2. EXPERIMENTAL PROCEDURE

BaSiON powder (Botterman et al., 2012) is embedded as an active ML component in a momentive Epikote RIM 135 epoxy matrix. The choice for the $\text{BaSi}_2\text{O}_2\text{N}_2:\text{Eu}$ material is mainly motivated by its strong light emission when stimulated in the elastic regime. The experiments for this study have all been obtained on thin BaSiON samples which have been optically charged by UV radiation sources. After charging, we respected a time period in order to reduce the strong, initial persistent luminescence. The BaSiON sample is then placed in water, after which it is insonified, leading to increased light emission (see Figure 1). The integrated light I , emitted by the BaSiON sample upon insonification, can be captured with a fiber coupled spectrometer (Ocean Optics QE6500) and a calibrated photometer (International Light Technologies ILT1700). To increase the contrast, the experiments take place in a darkened room. Figure 1 illustrates three cases in which ultrasound has been applied for different time periods after charging the BaSiON sample with UV light. During application of the ultrasound (indicated by the dashed lines), one can easily verify that the integrated light emission increases significantly.

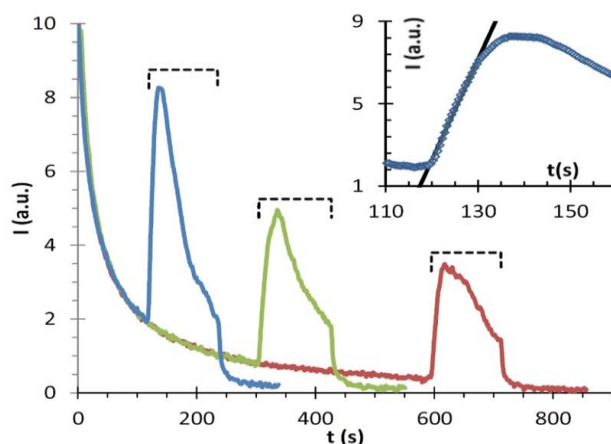


Figure 1: Measurement of the integrated emission intensity I when applying ultrasound (indicated by the dashed lines) at different times t . The inset shows an enlargement, along with a linear fit (dotted line) for the first 10 s.

The employed ultrasonic transducer (GYMNA 200 apparatus) has a circular active area of 470 mm², is immersed in water to enhance the transfer of ultrasound and is operated at a frequency of 3.3 MHz. The insonification distance z can be varied in order to obtain results in both near- and far-field of the transducer. The experimental setup is shown in Figure 2a. Figure 2b shows an example of a typically observed APL light pattern (captured with a standard digital camera) upon insonification of the BaSiON sample.

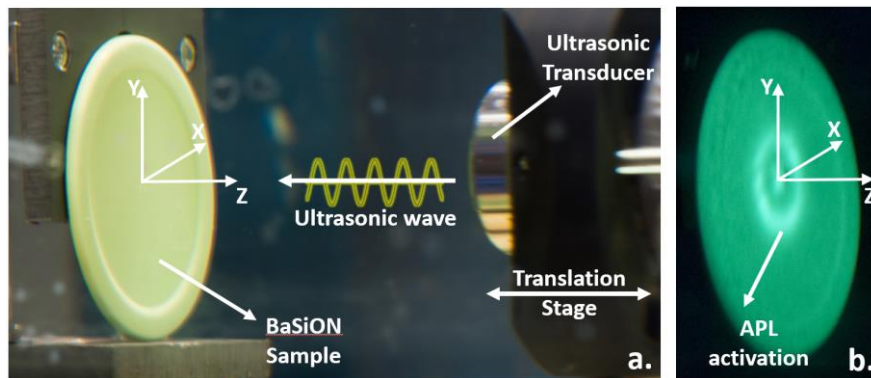


Figure 2: (a) Experimental setup and (b) example of APL activation.

3. RESULTS

3.1 Acoustic Power Sensor

First, it was investigated how the light emission varies with applied acoustic power. For this, the insonification distance z was fixed, while the applied acoustic power density was varied between 0 – 2 W/cm². Typically, this results in acoustic pressures up to 40 kPa in water. Figure 3a shows the recorded APL signal, with the dotted line indicating the time window during which ultrasound was applied. After integrating the light emission (between wavelengths of 450 and 550 nm, and between 210 and 250 seconds), one can easily verify the linear relationship between light emission intensity and applied acoustic power (Figure 3b). Hence, this indicates that the APL phenomenon can be used to devise a simple but effective acoustic power sensor.

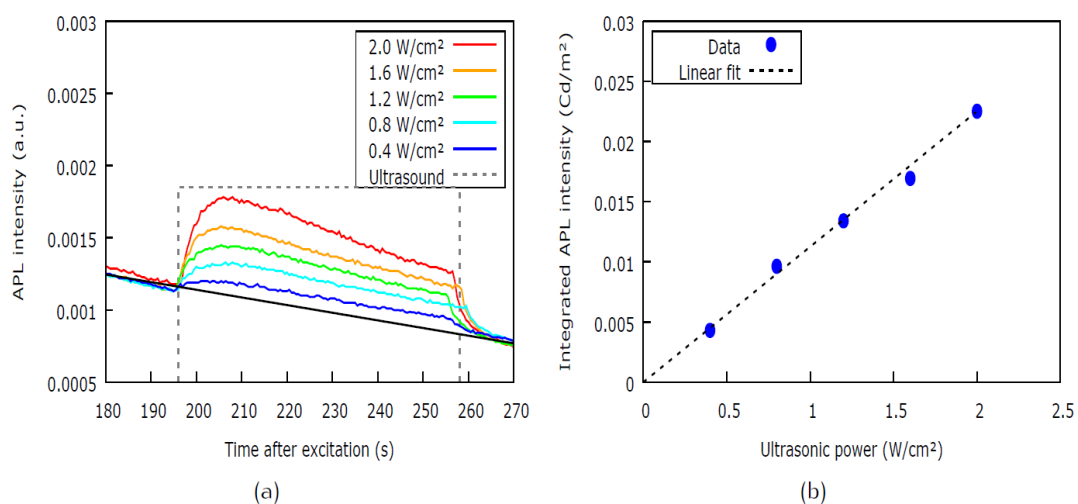


Figure 3: APL signal for different acoustic power (a) and linear relationship between integrated APL intensity and acoustic power (b).

3.2 Imaging Ultrasound

In Figure 2b one can easily verify that not only increased light emission is observed upon insonification, but that the APL signal has a specific geometrical shape. Moreover, when varying the insonification distance z we noted

that the geometrical pattern of the APL signal changes. This strongly suggests that the observed light pattern provides some insight on the local cross-sectional pressure distribution of the applied ultrasonic beam. Figure 4 shows the photographed APL light patterns for a range of insonification distances z at 2 W/cm^2 . Since the BaSiON samples were sufficiently thin, the photographs could be obtained in transmission (i.e. at the opposite side of insonification). A red-green-blue color scheme has been applied to the recorded images in order to enhance the visibility of features.

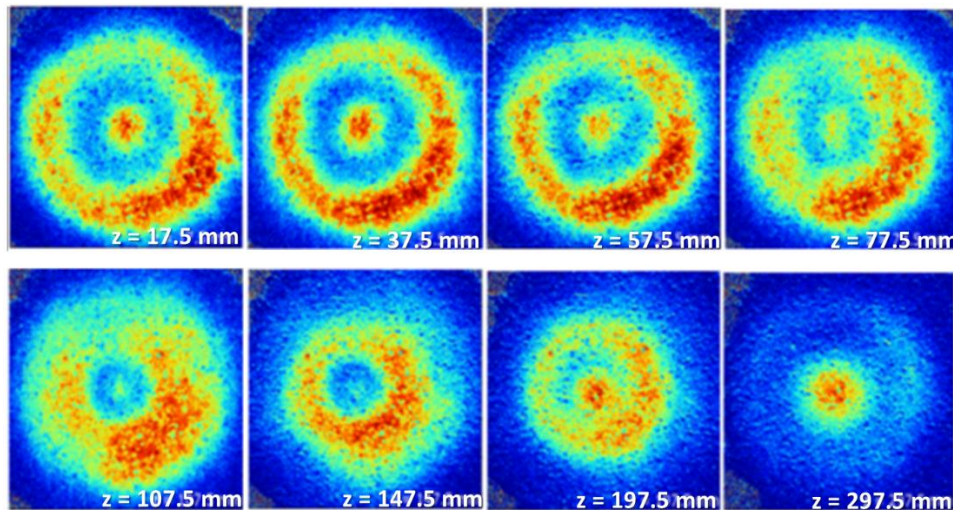


Figure 4: Photographed and digitized APL light emission intensity at various insonification distances z .

At short insonification distance z , one expects a representation of the vibrating surface of the transducer. The photograph obtained at $z \approx 17.5 \text{ mm}$ reveals an activated zone with global dimensions corresponding to the dimension of the employed transducer. However, instead of a uniform amplitude field, the activated zone has an annular shape with a disc inside. Clearly, the surface of the employed transducer vibrates with an inhomogeneous amplitude distribution, rather than a uniform amplitude profile. Comparison of the results obtained at different insonification distances z yields a change in geometry of the activated zone. For $z \leq 100 \text{ mm}$, the activated zone remains more or less similar, although the inner disc becomes less intense while the annular ring expands. At $z \approx 107.5 \text{ mm}$, the inner disc disappears leaving only a broad annular ring. At $z \approx 197.5 \text{ mm}$, the beam transforms back to the original distribution, i.e. a disc inside an annular ring. Finally, the pressure field evolves to a more or less Gaussian distribution at $z \approx 297.5 \text{ mm}$. It has been verified that the Gaussian shape remains for distances up to $z \approx 600 \text{ mm}$, while gradually spreading out. It is clear that the evolution of the cross-sectional pressure distribution as function of insonification distance z may be understood in terms of near- and far-field characteristics of a harmonically driven circular radiator.

One can also observe angular variations in the APL images, which cannot be linked to the diffractive nature of a bounded beam, nor to the geometry of the circular transducer. We have performed further experiments with different BaSiON samples, yielding the same results. Hence, the angular features are not induced by an inhomogeneous distribution of the dispersed luminescent powder. Consequently, small deviations in the radiation field of the transducer are most likely the cause of the angular variation in the APL signal. One possible origin for this may be the inappropriate fixation of the piezoelectric crystal in its housing, thus causing a spatially distorted and non-uniform vibration amplitude.

In order to confirm the APL results, we numerically reconstructed the radiation field according to the holographic principle on the basis of a fast Fourier transform beam propagation model (FFT-BPM) (Goodman, 1996). The transducer is modelled as a circular radiator having an amplitude distribution according to (with x, y in mm):

$$A(x, y, z = 0) = \begin{cases} 0 & 12.2 < \sqrt{x^2 + y^2} \\ 1 & 5.5 \leq \sqrt{x^2 + y^2} \leq 12.2 \\ 0 & 3.5 < \sqrt{x^2 + y^2} < 5.5 \\ 1 & \sqrt{x^2 + y^2} \leq 3.5 \end{cases}$$

This amplitude distribution can be considered as a simplified model for the true amplitude profile at the transducer’s surface. The phase is assumed to be uniform over the transducer’s surface. The numerical source is discretized in steps of $\Delta x = \Delta y = 0.02$ mm, oscillating at a frequency $f = 3.3$ MHz. The surrounding medium is modelled as water with density $\rho = 1000$ kg/m³ and wave speed $c = 1480$ m/s . After transforming (2D fast Fourier scheme) the pressure field to spatial frequency domain (k_x, k_y) , the result is multiplied with the free-space propagator $\exp(ik_z z)$, with $k_z = \sqrt{k^2 - k_x^2 - k_y^2}$ the wave number in z-direction and z the propagation distance. Application of the inverse Fourier transform then results into a representation of the acoustic beam in real space, which is propagated over a distance z . The periodic nature of the fast Fourier transform however results in reflections at the boundary of the numerical domain, which becomes especially cumbersome for large propagation distances. To avoid these interfering reflections without enlarging the size of the numerical domain, the acoustic beam is incrementally propagated in steps of $\Delta z = 1$ mm while applying a damping function D , in real space, to absorb the energy at the boundaries of the numerical domain:

$$D(x, y) = \exp\left(-\left(\frac{\sqrt{2\sqrt{x^2 + y^2}}}{0.97 \cdot W}\right)^{50}\right)$$

with W the size of the numerical domain.

The computed beam pattern in the YZ-plane is shown in Figure 5a. One can readily identify near-field features, until the far-field ($z \approx 250$ mm) emerges as a Gaussian-like amplitude distribution. Cross-sectional views at various distances z are shown in Figure 5b. In Figure 5c, the corresponding APL images are listed for the respective z -values. It may be clear that good agreement is found.

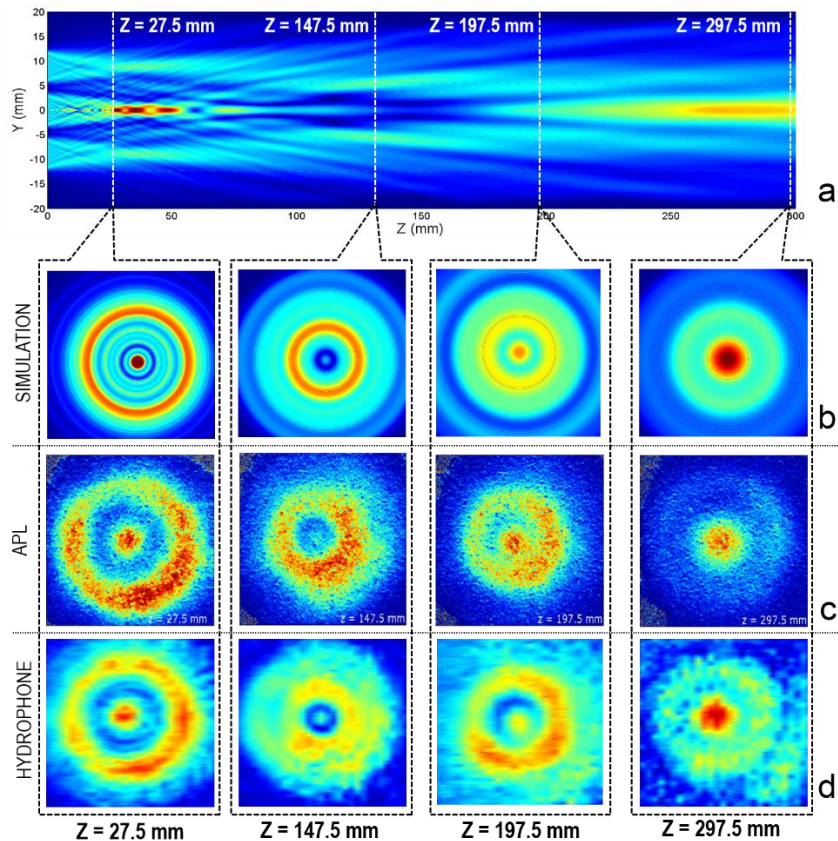


Figure 5: Simulated radiation field in YZ-plane (a), and XY cross-sectional views at various distances z : Simulation (b), APL experiment (c) and scanning hydrophone experiment (d).

Finally, we also recorded several cross-section of the radiation field by means of scanning hydrophone experiments. The XY-plane is scanned (spatial resolution of 0.25 mm) with a calibrated ONDA HGL-0400 needle hydrophone at various distances z . The ultrasonic amplitude is acquired with the USIP40 (General Electric) apparatus at sampling frequency of 400 MHz. Typically, one such experiment takes 30 minutes, which is in sharp contrast with the fast APL imaging (order of seconds for the actual measurement). The results are shown in Figure 5d for the selected insonification distances z . One can readily identify the presence of the radial and angular distribution, which we earlier linked to diffractive properties of the bounded beam on the one hand and to imperfections in the transducer design on the other hand. The transition of the cross-sectional geometry at the different distances z is in excellent agreement with both simulation and APL results.

3.3 Towards Acoustic Frequencies

APL experiments have also been performed at acoustic frequencies using lead zirconium titanate (PZT) patches which are directly bonded to BaSiON (as well as other piezoluminescent phosphors) samples using phenyl salicylate. The PZT patches are driven in the kHz range by a wave generator (Tektronix AFG 3021B) coupled to a voltage multiplier (Falco WMA300). Electrical input voltage between 1-300 V_{pp} is considered. Our preliminary results indicate that also kHz waves trigger the APL phenomenon. At low voltage input (1-50 V_{pp}) however the PZT patches do not lead to strong APL signal, which is in clear contrast to the excellent results obtained with the MHz transducer. These first results indicate that the acoustic power generated by the PZT patches is simply not sufficient to trigger the APL phenomenon efficiently (see Figure 6). The observed increase in light intensity barely exceeds the afterglow curve, indicating that only a limited amount of APL is involved, and that the process is dominated by thermal detrapping.

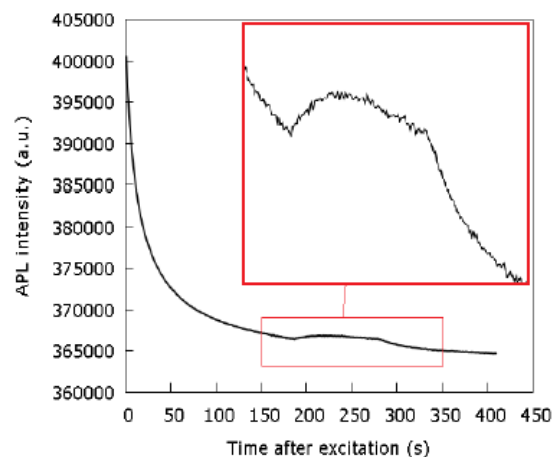


Figure 6: APL signal obtained for PZT patch at 20 kHz and input voltage of 50 V_{pp} .

The logic step would be to increase the applied voltage on the PZT in order to induce higher acoustic power, and as a consequence to increase the APL signal with respect to the signal associated with thermal detrapping. By increasing the input voltage to 50 - 300 V_{pp} , a clear increase in light emission was observed. However, by doing so we noted that also secondary effects are induced in the employed PZT patches, which compromise the APL measurements. First of all, we found that the used PZT patches behave nonlinear at high voltage input. This is illustrated in Figure 7 showing the vibrational response in frequency domain (measured with a laser Doppler vibrometer) of a PZT driven at a frequency of 5 kHz and voltage input of 200 V_{pp} . Besides the clear spike at the input frequency of $f = 5$ kHz, one can clearly discern several super- and subharmonics revealing the nonlinear behavior of the PZT patch when driven at high voltage. This nonlinear response of the PZT's became pronounced for voltages higher than 50 V_{pp} .

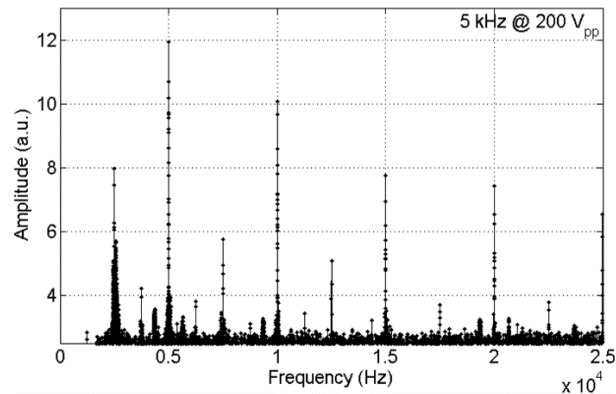


Figure 7: Vibrational response of a PZT patch driven at 5 kHz and 200 V_{pp}.

Apart from nonlinearity in the response of the PZT patch, we also noted some heating when applying voltages higher than 50 V_{pp}. The temperature evolution of the PZT patch has been monitored by a thermographic camera for different applied voltages. The results are shown in Figure 8, revealing that considerable heat is produced when driving the PZT at voltages higher than 50 V_{pp}. Obviously, the generation of heat compromises our APL measurements as thermoluminescent processes come into play.

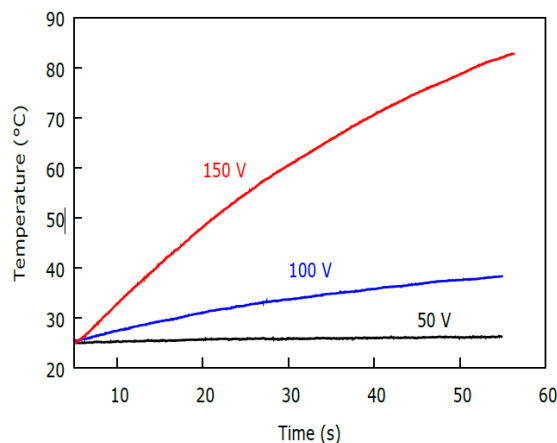


Figure 8: Temperature evaluation of PZT patch when driven at 20 kHz and different voltages.

Hence, these preliminary results indicate that APL can be triggered in the acoustic regime, but with the current low power PZT patches the efficiency is not satisfactory. In addition, the employed PZT patches show secondary effects which compromise the APL measurements. Currently we are investigating different excitation methods in the kHz range in order to overcome the aforementioned problems of the PZT patches regarding nonlinearity and heating. As such, we hope to apply the APL phenomenon for various applications in the acoustic frequency region.

4. CONCLUSIONS

This paper introduced the phenomenon of acoustically induced piezoluminescence (APL). It was shown that the APL effect provides opportunities for the development of a simple but effective acoustic power sensor. Further, the APL phenomenon has been employed to obtain cross-sectional images of the pressure field of an ultrasonic beam ($f = 3.3$ MHz) in real-time. Combining many of such cross-sections then yields a 3D spatial representation of the pressure distribution of an ultrasonic field in both near- and far-field. Good agreement was found between the reconstructed pressure distributions through APL on the one hand, and both simulation and conventional scanning hydrophone experiments on the other hand. Compared to conventional methods, APL imaging of ultrasonic beams has the clear advantage that it is simple, cheap and fast. Finally, preliminary experiments have been presented which

indicate that the APL phenomenon is equally valid for acoustic frequencies. Unfortunately, secondary effects in the employed PZT actuators compromised the APL signals, making a clear interpretation difficult. Current research focuses on implementing alternative excitation methods in the kHz range in order to isolate the APL signals from secondary phenomena, and to identify the underlying physical processes of APL.

ACKNOWLEDGEMENTS

Mathias Kersemans acknowledges the financial support of Fonds voor Wetenschappelijk Onderzoek FWO-Vlaanderen (grant G012010N) and Bijzonder Onderzoeksfonds BOF (grant BOF.PDO.2015.0028.01). The authors further acknowledge the BOF-GOA Enclose project.

REFERENCES

- BACON, F. 1605. *The advancement of learning*, Oxford.
- BOTTERMAN, J., VAN DEN ECKHOUT, K., DE BAERE, I., POELMAN, D. & SMET, P. F. 2012. Mechanoluminescence in BaSi₂O₂N₂:Eu. *Acta Materialia*, 60, 5494-5500.
- BRITO, H. F., HOLSA, J., LAAMANEN, T., LASTUSAARI, M., MALKAMAKI, M. & RODRIGUES, L. C. V. 2012. Persistent luminescence mechanisms: human imagination at work. *Optical Materials Express*, 2, 371-381.
- CHANDRA, V. K., CHANDRA, B. P. & JHA, P. 2013. Strong luminescence induced by elastic deformation of piezoelectric crystals. *Applied Physics Letters*, 102, 241105.
- GOODMAN, J. W. 1996. *Introduction to Fourier Optics*, New York, McGraw-Hill.
- KERSEMANS, M., SMET, P., LAMMENS, N., DEGRIECK, J. & VAN PAEPEGEM, W. 2015. Fast reconstruction of a bounded ultrasonic beam using acoustically induced piezo-luminescence. *Applied Physics Letters*, 107.
- KIM, J. S., KWON, Y. N., SHIN, N. & SOHN, K. S. 2007. Mechanoluminescent SrAl₂O₄ : Eu, Dy phosphor for use in visualization of quasidynamic crack propagation. *Applied Physics Letters*, 90.
- MATSUZAWA, T., AOKI, Y., TAKEUCHI, N. & MURAYAMA, Y. 1996. New long phosphorescent phosphor with high brightness, SrAl₂O₄:Eu²⁺,Dy³⁺. *Journal of the Electrochemical Society*, 143, 2670-2673.
- TERASAKI, N., YAMADA, H. & XU, C. N. 2013. Ultrasonic wave induced mechanoluminescence and its application for photocatalysis as ubiquitous light source. *Catalysis Today*, 201, 203-208.
- TIMILSINA, S., LEE, K. H., JANG, I. Y. & KIM, J. S. 2013. Mechanoluminescent determination of the mode I stress intensity factor in SrAl₂O₄:Eu²⁺,Dy³⁺. *Acta Materialia*, 61, 7197-7206.
- VAN DEN ECKHOUT, K., BOS, A. J. J., POELMAN, D. & SMET, P. F. 2013. Revealing trap depth distributions in persistent phosphors. *Physical Review B*, 87, 045126.
- VAN DEN ECKHOUT, K., SMET, P. F. & POELMAN, D. 2010. Persistent Luminescence in Eu²⁺-Doped Compounds: A Review. *Materials*, 3, 2536-2566.
- WANG, X., ZHANG, H., YU, R., DONG, L., PENG, D., ZHANG, A., ZHANG, Y., LIU, H., PAN, C. & WANG, Z. L. 2015. Dynamic Pressure Mapping of Personalized Handwriting by a Flexible Sensor Matrix Based on the Mechanoluminescence Process. *Advanced Materials*, 27, 2324-2331.
- XU, C. N., ZHENG, X. G., AKIYAMA, M., NONAKA, K. & WATANABE, T. 2000. Dynamic visualization of stress distribution by mechanoluminescence image. *Applied Physics Letters*, 76, 179-181.
- ZHAN, T., XU, C.-N., FUKUDA, O., YAMADA, H. & LI, C. 2011. Direct visualization of ultrasonic power distribution using mechanoluminescent film. *Ultrasonics Sonochemistry*, 18, 436-439.
- ZHANG, J.-C., XU, C.-N., KAMIMURA, S., TERASAWA, Y., YAMADA, H. & WANG, X. 2013. An intense elasto-mechanoluminescence material CaZnOS:Mn²⁺ for sensing and imaging multiple mechanical stresses. *Optics Express*, 21, 12976-12986.